Assignments, Secondary Structure, Global Fold, and Dynamics of Chemotaxis Y Protein Using Three- and Four-Dimensional Heteronuclear (^{13}C,^{15}N) NMR Spectroscopy†

Franklin J. Moy,*,‡,§ David F. Lowry,‖ Philip Matsumura,⊥ Frederick W. Dahlquist,‖ James E. Krywko,‡ and Peter J. Domaille*,‡

Chemical & Physical Sciences, The DuPont Merck Pharmaceutical Company, Wilmington, Delaware 19880-0328, Institute of Molecular Biology and Department of Chemistry, University of Oregon, Eugene, Oregon 97403, and Department of Microbiology and Immunology, University of Illinois, Chicago, Illinois 60612

Received April 5, 1994; Revised Manuscript Received June 10, 1994®

ABSTRACT: NMR spectroscopy has been used to study recombinant *Escherichia coli* CheY, a 128-residue protein involved in regulating bacterial chemotaxis. Heteronuclear three- and four-dimensional (3D and 4D) experiments have provided sequence-specific resonance assignments and quantitation of short-, medium-, and long-range distance restraints from nuclear Overhauser enhancement (NOE) intensities. These distance restraints were further supplemented with measurements of three-bond scalar coupling constants to define the local dihedral angles, and with the identification of amide protons undergoing slow solvent exchange from which hydrogen-bonding patterns were identified. The current model structure shows the same global fold of CheY as existing X-ray structures (Volz & Matsumura, 1991; Stock *et al.* 1993) with a $(\beta/\alpha)_5$ motif of five parallel β-strands at the central core surrounded by three α-helices on one face and with two on the opposite side. Heteronuclear ^{15}N–^{1}H relaxation experiments are interpreted to show portions of the protein structure in the Mg^{2+} binding loop are ill-defined because of slow motion (chemical exchange) on the NMR time scale. Moreover, the presence of Mg^{2+} disrupts the salt bridge between the highly conserved Lys-109 and Asp-57, the site of phosphorylation.

Two-component regulatory systems play important roles in allowing bacteria to respond to a variety of environmental signals. The two components include a transmitter module histidyl kinase and a receiver module protein in which an aspartate residue serves as the phosphorylation site. Changes in the environment result in changes in the phosphorylation level of the receiver domain that then cause changes in gene expression or other physiological events associated with the particular signal transduction pathway in question. Recent excellent reviews (Stock *et al.*, 199; Volz, 1993) have described the cytoplasmic family of Che proteins from *Escherichia coli* as a model for intracellular signal transduction. The CheY[1] protein is one of the best understood of the receiver domain family. It functions as a molecular switch in regulating bacterial chemotaxis via its phosphorylation-activated response; in the phosphorylated form it binds to the flagellar motor and causes the bacteria to tumble and change their direction of swimming. When dephosphorylated the protein is inactivated and returns to its resting state. The biochemistry of this process is understood at the molecular level: CheY catalyzes the transfer of a phosphoryl group from His-48 of the protein kinase CheA to Asp-57 of CheY. The active site contains a Mg^{2+} ion and two additional carboxylates (Asp-12 and Asp-13) within the binding pocket. During phosphorylation the D57–Mg^{2+} coordination in CheY is disrupted, with the metal now directly coordinating with the phosphate, resulting in considerable restructuring of the active site as evidenced by the large NMR chemical shift changes occurring in the protein backbone (Lowry *et al.*, 1994).

As part of an ongoing study aimed at unraveling the details of these structural changes of CheY in solution, we report here the NMR signal assignments and a model structure of dephosphorylated CheY in the presence of Mg^{2+}. The assignments are made on the basis of three- and four-dimensional heteronuclear triple-resonance experiments based on scalar couplings. No reference to existing X-ray structures was made in the assignment process because changes might result from crystal packing and inclusion of other counterions (Volz, 1993). A recent report (Kraulis *et al.*, 1994) of the NMR solution structure of p21 ras.GDP, an analogous eukaryotic signal transduction protein in the inactive state, showed differences from the X-ray structures in the functionally important regions of the structure. In hindsight, because of limited numbers of NOE's due to Mg^{2+} chemical exchange in certain regions of CheY, our structure is insuffiently well determined to make similar in-depth comparisons.

† D.F.L. is supported by a Cancer Research Fund of the Damon Runyon–Walter Winchell Foundation Fellowship DRG-1195. F.W.D. was supported by NIH (Grant GM33677).

* To whom correspondence should be addressed.

‡ The DuPont Merck Pharmaceutical Co.

§ Present address: American Cyanamid Co., Medical Research Division, Lederle Laboratories, Pearl River, NY 10965.

‖ University of Oregon.

⊥ University of Illinois.

® Abstract published in *Advance ACS Abstracts,* August 1, 1994.

[1] Abbreviations: CheY, chemotaxis Y protein; PMSF, phenylmethanesulfonyl fluoride; EDTA, sodium salt of ethylenediaminetetraacetic acid; Tris, tris(hydroxymethyl)aminomethane; MES, 2-(*N*-morpholino)ethanesulfonic acid; IPTG, isopropyl β-D-thiogalactopyranoside; NMR, nuclear magnetic resonance; NOE, nuclear Overhauser effect; NOESY, nuclear Overhauser enhancement spectroscopy; HOHAHA, homonuclear Hartmann–Hahn; HMQC, heteronuclear multiple quantum coherence; HSQC, heteronuclear single-quantum coherence; CT, constant time; 2D, 3D, and 4D, two-, three-, and four-dimensional NMR; 3D NOESY-HMQC, 3D NMR experiment combining NOESY and HMQC; HNNCAHA, H^N to ^{15}N to $^{13}C^\alpha$ to H^α intraresidue correlation; HCA(CO)NNH, H^α to $^{13}C^\alpha$ sequential (via carbonyl carbon) to ^{15}N to H^N correlation; HNCA, H^N to ^{15}N to $^{13}C^\alpha$ correlation; HNHB, H^N to ^{15}N to H^β correlation; TPPI, time-proportional phase incrementation; T_2', the arithmetic mean of the zero quantum and double quantum relaxation times, SA, simulated annealing; rms, root mean square; X-PLOR, computer program for macromolecular simulation.

0006-2960/94/0433-10731$04.50/0

During preparation of this paper a partial NMR assignment of a CheY variant has appeared (Bruix *et al.*, 1993). In this work the N-terminal three residues of the native sequence (Met-Ala-Asp...) had been modified (Met-Arg-Ser-Asp...) in the recombinant form studied and the protein did not contain Mg^{2+}. Since Mg^{2+} is required for phosphorylation, and a full sequence-specific assignment of the NMR signals is a necessary prerequisite for understanding the changes which accompany it, this work has focused on the Mg^{2+} apo form. Additionally, a new pair of crystal structures of CheY in the presence and absence of Mg^{2+} has been reported (Stock *et al.*, 1993). We show that Mg^{2+} binding has a substantial effect on the NMR spectra, and moreover, the dynamics of metal exchange influences the spectra and structure. Heteronuclear $^{15}N\{^1H\}$ NOE and ^{15}N T_1 and T_2 measurements are used to account for the less well characterized regions of the structure and are attributed to Mg^{2+} exchange.

MATERIALS AND METHODS

Production of Recombinant $^{13}C/^{15}N$-Labeled CheY. CheY labeled with ^{15}N and ^{13}C was overexpressed and purified as described in Matsumura *et al.* (1984) except cultures were grown in M9 minimal medium with [^{15}N]ammonium chloride and [^{13}C]glucose as the sole sources of nitrogen and carbon, respectively. Overexpression of CheY results in posttranslational cleavage of the amino-terminal methionine; hence, our protein numbering scheme starts at Ala-2. The purified protein was stored as an ammonium sulfate precipitate. NMR samples were prepared by pelleting the precipitate (35 mg) by centrifuging at 7840*g*, 4 °C for 15 min. The pellet was resuspended in 10 mL of 50 mM Tris, pH 8.0, and dialyzed first against Tris at pH 8.0 and then against 50 mM sodium phosphate, pH 6.2, and 5 mM magnesium chloride; final pH of the dialysate was 6.6. Since two separate $^{13}C/^{15}N$ uniform labeled samples were needed, one dissolved in 90% H_2O/10% D_2O for use in triple-resonance experiments requiring H^N detection, and the other in 99.8% D_2O for experiments involving nonexchangeable protons, the sample was divided into two portions and each concentrated to 500 μL (Microsep centrifugal microconcentrator, Filtron Technology Corp.). The D_2O sample was further exchanged by spinning through a G-25 spin column; the final measured pH 6.8 is uncorrected for isotope effects. Using a spin column rather than repeated cycles of lyophilization and incubation with D_2O results in a substantial residual HOD signal. Sample concentrations were 1.9 mM calculated from the absorbance at 280 nm using a molar extinction coefficient of 8250.

Selective ^{15}N-Labeling of CheY. In addition to a uniformly ^{15}N-labeled sample in 90% H_2O/10% D_2O, seven samples with specific incorporation of ^{15}N into alanine, leucine, lysine, aspartic acid/asparagine, valine, methionine, and glycine were also examined for the purpose of identifying (H^N, ^{15}N) resonances which shift upon phosphorylation (Lowry *et al.*, 1994) or which were not evident at lower Mg^{2+} concentration. These proteins were overexpressed using defined media and suitable auxotrophs as described elsewhere (Muchmore *et al.*, 1989). Cells were induced at 0.5 A_{600} with 1 mM IPTG, with growth continuing for varying periods (strain dependent) until harvest. The cells from a 1-L growth were resuspended in 60 mL of 50 mM Tris, pH 7.9, 1 mM EDTA, and 0.2 M PMSF and mildly sonicated at 4 °C; cell debris was removed by centrifugation at 27000*g*, 4 °C for 30 min. The supernatant was dialyzed against 50 mM MES, pH 5.3, and 0.2 mM PMSF and chromatographed on DE52 (Whatman), 300-mL linear 0–50 mM sodium chloride gradient in MES buffer, 1.8 mm^2 × 9 mm bed volume. Fractions containing CheY were pooled, dialyzed against 5 mM Tris, pH 7.5, and chromatographed on DE52 5 mM Tris, pH 7.5, 300-mL linear 0–400 mM sodium chloride gradient, 1.8 mm^2 × 9 mm bed volume. Fractions were again pooled, dialyzed against 50 mM Tris, pH 7.9, 1 mM EDTA, and 0.02% (by weight) sodium azide, and batch eluted off cibacron blue (Sigma) with 2 M sodium chloride. Pure CheY was dialyzed against 100 mM sodium phosphate, pH 7.7, 0.02% sodium azide, and magnesium chloride added to a final concentration of approximately 5 mM. Various samples for NMR spectroscopy were prepared as above at concentrations of 1–4 mM, pH 6.75 ± 0.05, containing 50–100 mM sodium phosphate, 4–5 mM magnesium chloride, and 0.02% (by weight) sodium azide.

NMR Data Collection. (1) General. All spectra were recorded at 30 °C on Bruker AMX600 spectrometers using either a triple-resonance $^1H/^{13}C/^{15}N$ probe or a double-resonance inverse probe. The NMR data for CheY are based on the following series of experiments: 2D ^1H–^{15}N HSQC (Bodenhausen & Ruben, 1980), 2D ^1H–^{15}N *J*-HSQC (Neri *et al.*, 1990; Billeter *et al.*, 1992), 2D heteronuclear $^{15}N\{^1H\}$ NOE and 2D ^1H–^{15}N T_1 and T_2 (Barbato *et al.*, 1992), 2D ^1H–^{13}C HSQC (Vuister & Bax, 1992), 3D ^{15}N-edited NOESY-HMQC (Marion *et al.*, 1989a; Zuiderweg & Fesik, 1989), ^{13}C-edited NOESY-HMQC (Ikura *et al.*, 1990a), 3D ^1H–^{15}N HMQC-NOESY-HMQC (Ikura *et al.*, 1990b), 3D ^{15}N-edited HOHAHA (Marion *et al.*, 1989a; Clore & Gronenborn, 1991), 3D ^{15}N-edited HNHB (Archer *et al.*, 1991), 3D coupled HNCA (Seip *et al.*, 1992; Gorlach *et al.*, 1993), 3D HCCH-COSY (Bax *et al.*, 1990a; Ikura *et al.*, 1991), 3D HCCH-TOCSY (Bax *et al.*, 1990b), 4D $^{13}C/^{15}N$-edited NOESY (Kay *et al.*, 1990), 4D $^{13}C/^{13}C$-edited NOESY (Clore *et al.*, 1991; Vuister *et al.*, 1993), 4D HNNCAHA (Boucher *et al.*, 1992b; Kay *et al.*, 1992; Olejniczak *et al.*, 1992; Clubb *et al.*, 1992), and 4D HCA(CO)NNH (Boucher *et al.*, 1992a).

Data collection parameters are collected below in the section in which they were used. In general, water suppression, in experiments which involve preparation of ^{15}N magnetization via INEPT transfer from H^N, was carried out with a 1.0–1.5-ms spin-lock pulse (Messerle *et al.*, 1989) with only slight presaturation (*ca.* 5–10 Hz) to improve the dynamic range. Most spectra are collected with reduced spectral widths in the indirectly detected dimensions with either States (States *et al.*, 1982) or States-TPPI hypercomplex (Marion *et al.*, 1989b) phase incrementation; this causes signals which fall outside of the spectral window to alias. Initial time delays in these dimensions either were set to allow aliasing to occur with positive/negative sign discrimination of even/odd alias numbers (−180° linear phase correction) or were delayed by a full dwell time causing no sign differentiation. Whenever possible, appropriate refocusing delays were incorporated into pulse sequences to allow spectra without any phase correction.

Data were processed in the acquisition dimension using conventional Fourier transforms in FELIX 1.1 (Hare Research, BioSym Technologies) after time domain convolution difference water reduction (Marion *et al.*, 1989c) and apodization with a shifted sine bell or squared sine bell window function. Processing in the indirect dimensions utilized either FELIX Fourier transforms or 1D and 2D Maximum Entropy Method algorithms described in earlier publications (Laue *et al.*, 1986; Boucher *et al.* 1992a). Final spectra always used FELIX format for display, but chemical shift data were analyzed manually and sorted with in-house software. Time-dependent intensity data, such as that encountered in T_1, T_2,

heteronuclear NOE, and *J*-modulated HSQC, were quantitated in FELIX 1.1 or 2.1 but were externally fit using our own programs.

(2) Sequence-Specific Residue Assignments. The backbone nuclei (H^N, ^{15}N, C^α, H^α) sequential assignments were based on the constant-time 4D HNNCAHA and HCA(CO)NNH experiments using the same strategy described previously (Boucher *et al.*, 1992a,b; Campbell-Burk *et al.*, 1992). Both the 4D HNNCAHA and 4D HCA(CO)NNH spectra were recorded with 16 scans per increment, resulting in a total measuring time of *ca.* 97 h for each. 2D versions of the HNNCAHA and HCA(CO)NNH were also recorded with transfer parameters optimized for glycine residues (Campbell-Burk *et al.*, 1992). Acquisition times in $t1$ ($^1H^\alpha$), $t2$ (^{13}C), $t3$ (^{15}N), and $t4$($^1H^N$) were 22.1, 3.2, 9.8, and 63.5 ms, respectively, with the appropriate carrier frequencies of 4.72 ppm ($F1$, $F4$), 57.1 ppm ($F2$), and 117.8 ppm ($F3$). The final size of the matrices (64 × 64 × 64 × 512) results in a digital resolution for $F1$ ($^1H^\alpha$), $F2$ (^{13}C), $F3$ (^{15}N), and $F4$ ($^1H^N$) of 22.6, 39.0, 12.8, and 7.9 Hz/pt, respectively.

Side-chain assignments mainly utilized the 3D HCCH-COSY and -TOCSY experiments, using the H^α, C^α coordinates as starting points. Details of specific assignment strategies are contained in the Results and Discussion section. Both the 3D HCCH-COSY and -TOCSY [DIPSI-2 (Shaka *et al.*, 1988), mixing time 24 ms] spectra were recorded with 16 scans per increment and total measuring times of *ca.* 84 h. The acquisition times in $t1$ (^1H), $t2$ (^{13}C), and $t3$ (^1H) were 19.2, 8.0, and 63.5 ms, respectively, with the carrier frequencies centered at 4.72 ppm ($F1$, $F3$) and 46.5 ppm ($F2$). Digital resolution in the final 512 × 128 × 512 matrices were 13.0 Hz/pt ($F1$), 31.3 Hz/pt ($F2$), and 7.9 Hz/pt ($F3$).

(3) NOE Assignments and Determination of Interproton Distance Restraints. NOE's were assigned from several 3D and 4D heteronuclear-edited NOESY spectra recorded with mixing times ranging from 100 to 120 ms. To aid in the identification of weaker peaks, one 3D ^{15}N-edited NOESY was collected with a mixing time of 150 ms. The 3D ^{15}N-edited NOESY spectra were recorded with 16 scans per increment while a 3D ^1H–^{15}N HMQC-NOESY-HMQC spectrum was recorded with 32 scans per increment. The spectral widths in both ^1H dimensions were 8064.52 Hz while both ^{15}N dimensions were 819.67 Hz. The ^1H carrier was positioned on the H_2O resonance at 4.72 ppm with slight presaturation and a SCUBA (Brown *et al.*, 1988) recovery period while the ^{15}N carrier was centered at 117.8 ppm. Acquisition times were 39.0 ms for ^{15}N and 15.9 ms for ^1H ($t1$) and 129 ms for ^1H ($t3$). Final digital resolution was 6.4 Hz/pt for ^{15}N, 3.9 Hz/pt for ^1H ($F3$), and 15.8 Hz/pt for $^1H^N$ ($F1$).

The 3D ^{13}C-edited NOESY-HMQC spectrum (mixing time 100 ms) was recorded with 32 scans per increment and a total measuring time of 96 h. The spectral widths in both ^1H dimensions were 8064.52 Hz with the carrier at 4.72 ppm; the ^{13}C carrier was placed in a clear region of the spectrum at 46.5 ppm, and phase-sensitive spectra were acquired with States hypercomplex phase incrementation so any residual axial artifacts would occur here rather than at the edge of the severely aliased ^{13}C dimension where there are a substantial number of cross-peaks. The acquisition times in $t1$ (^1H), $t2$ (^{13}C), and $t3$ (^1H) were 15.9, 8.0, and 63.5 ms, respectively, with final digital resolution of $F1$, $F3$ (15.9 Hz/pt), and $F2$ (31.3 Hz/pt).

The 4D ^{13}C/^{13}C-edited NOESY spectrum (mixing time 100 ms) was recorded with 4 transients per increment and a total measuring time of 124 h. The acquisition times $t1$ and $t3$ (^{13}C) were 2.5 ms (10 complex increments) and 12.8 and 31.7 ms in $t2$ (^1H) and $t4$ (^1H), respectively. Carrier positions were identical to the 3D ^{13}C-edited NOESY and States phase incrementation used for the same reasons cited above in $t1$ and $t3$. The final digital resolution in the 64 × 128 × 64 × 256 matrix was 62.5 Hz/pt ($F1$ and $F3$), 39.1 Hz/pt ($F2$), and 15.8 Hz/pt ($F4$).

The 4D ^{13}C/^{15}N-edited NOESY spectrum (mixing time 120 ms) was also recorded with 4 transients per increment and a total measuring time of 117 h. Acquisition times in $t1$ (^1H), $t2$ (^{13}C), $t3$ (^{15}N), and $t4$ ($^1H^N$) were 12.8, 5.0, 9.8, and 63.5 ms, respectively, with the ^1H, ^{13}C, and ^{15}N carrier frequencies set at 4.72, 46.5, and 117.8 ppm, respectively.

Cross-peaks in all NOESY spectra were picked in FELIX and then assigned by searching an assignment database using in-house software. Ambiguous assignments, based on overlap of chemical shifts within certain tolerance margins, were deferred until after initial structure calculations were completed. Upper-bound distance restraints in H_2O spectra were calibrated using the strongest sequential H^α_i–H^N_{i+1} NOE's in the spectra which occur in regular regions of parallel β-sheet assuming a distance of 2.2 Å (Billeter *et al.*, 1982). The NOE's involving amide protons were classified into strong, medium, and weak corresponding to distance restraints of 1.8–2.7, 1.8–3.5, and 1.8–5.0 Å, respectively. For the ^{13}C-edited NOESY experiments the NOE's were all conservatively classified as weak corresponding to a distance restraints of 1.8–5.0 Å. Pseudo atom corrections (Wüthrich *et al.*, 1983; Wüthrich, 1986) were added to the upper-bound distance restraints derived from the NOE data in cases where stereospecific assignments were not made. For the situation wherein both NOE's between given protons of a single methylene group or to both methyl groups of valine and leucine could be identified, the longer of the two distance constraints was used (Montelione *et al.*, 1992; Moy *et al.*, 1993).

(4) Determination of Dihedral Angle Restraints. Once the (^1H, ^{15}N) assignments were known, a series of 2D ^1H–^{15}N J-modulated HSQC experiments were collected (Neri *et al.*, 1990; Billeter *et al.*, 1992) to determine $^3J(H^N–H^\alpha)$ coupling constants and provide ϕ torsion angle restraints. In this experiment, the HSQC pulse sequence is followed by a delay period, τ_2, during which the $^1J(^{15}N–H^N)$ coupling is refocused, and the $^3J(H^N–H^\alpha)$ coupling modulates multiple-quantum $^{15}N–H^N$ coherence. These spectra were reduced to the same spectral widths used for all ^1H–^{15}N correlation measurements, namely, 4032.26 Hz ($F2$, ^1H) and 819.67 Hz ($F1$, ^{15}N), but for optimum $F2$ base line the acquired data were overdigitized at a spectral/filter width of 16 129 Hz and processed in $F2$ to discard the region devoid of signal. Acquisition times used were 127 ms ($t2$) and 39 ms ($t1$) with a series of τ_2 values of 9.2, 30, 50, 56, 63, 71, 83, 100, 125, and 167 ms. Nonlinear fits (Press *et al.*, 1989) to the τ_2-dependent cross-peak volume, $V(\tau_2) = A[\cos(\pi J\tau_1)\cos(\pi J\tau_2) - 0.5\sin(\pi J\tau_1)\sin(\pi J\tau_2)]\exp(-\tau_2/T_2')$, were used to obtain the $^3J(H^N–H^\alpha)$ coupling constant and the apparent relaxation time, T_2' (Billeter *et al.*, 1992).

A 3D coupled HNCA experiment was also used to directly measure the $^3J(H^N–H^\alpha)$ coupling constants from the E.COSY pattern (Seip *et al.*, 1992; Gorlach *et al.*, 1993), providing an independent cross check and also additional values which were not obtained from the ^1H–^{15}N *J*-modulated HSQC experiments because of ^1H–^{15}N overlap. Acquisition times in $t1$ (^{15}N), $t2$ (^{13}C), and $t3$ (H^N) were 9.8, 12.0, and 254 ms, respectively, with the carrier frequencies set exactly the same

as the 4D HNNCAHA assignment experiment.

(5) Heteronuclear NOE and ^{15}N T_1 and T_2 Measurements. The heteronuclear NOE and T_1 and T_2 relaxation times were measured with the standard $^1H^N$ and ^{15}N spectral widths with maximum acquisition times of 127 ms ($t2$) and 78 ms ($t1$). Since the NOE measurement requires equilibrium ^{15}N magnetization for accurate quantitation, the recycle time was extended to more than 4 s and 64 transients per increment were acquired for suitable sensitivity. Both the T_1 and T_2 data were collected with 32 transients per increment; for T_1 we used inversion recovery times of 30, 50, 70, 110, 150, 190, 230, 310, 390, 500, 750, 1000, and 2000 ms while for T_2 the Carr–Purcell–Meiboom–Gill trains were 8, 16, 24, 32, 40, 56, 72, 88, 120, 144, 168, 192, 216, 248, and 280 ms in duration. T_1 and T_2 values were determined by a two-parameter nonlinear least-squares fit to the volume vs time profile, $V(t) = V_0 \exp(-t/T_n)$, using in-house software. NOE values were quantitated from the ratio of the intensity of the two spectra in the presence and absence of ^1H saturation, respectively.

(6) Hydrogen/Deuterium Exchange Measurements. Slowly exchanging H^N were measured by the rate of disappearance of ^1H–^{15}N cross-peaks in an HSQC spectrum recorded as a function of time after dissolving uniformly ^{15}N-labeled CheY in D_2O, at pH 6.75 and 30 °C. Spectra were acquired beginning at 6, 22, 38, 64, 96, 160, 288, and 416 min after dissolution.

Structure Calculations. (1) Initial Evaluation of NOESY Data. Structure calculations were carried out on a Silicon Graphics 480 processor using the program X-PLOR (Brunger, 1992; Kuszewski *et al.*, 1992). The protocol uses an initial distance geometry subembed step wherein the backbone atoms N, C^α, and C′ are embedded from n-dimensional distance space into Cartesian coordinate space (Havel *et al.*, 1983) and then followed by dynamical simulated annealing (Clore *et al.*, 1990). In the first round of the structure calculations 160 intraresidue, 185 sequential, and 196 medium- and long-range unambiguous NOE's and 68 ϕ torsion angles were used as restraints. Ten preliminary structures were computed, using a starting point of an extended structure, and all converged with no distance violations greater than 0.5 Å and no torsion angle violations greater than 5°. The extremes of these structures were than used as a distance filter to interpret additional NOESY cross-peaks which were judged as ambiguous in the first round. The additional NOE restraints resulting from this reiterative procedure were then merged to form a new restraint list. The hydrogen-bonding restraints were also introduced at this stage when both the donor and acceptor pair could be unambiguously identified from the family of structures.

(2) Final Structure Calculations. The final 46 simulated annealing (SA) structures, starting from 60 subembedded structures, were calculated with 1032 experimental NMR restraints. These comprised 852 approximate interproton distance restraints which were classified as follows: 158 intraresidue, 214 sequential interresidue ($|i - j| = 1$), 228 medium-range ($1 < |i - j| \leq 5$), and 252 long-range ($|i - j| > 5$). Included in the final structure calculations also were 44 ψ torsion angles which were identified in helical regions (Spera & Bax, 1991), 68 ϕ torsion angles from $^3J(H^N–H^\alpha)$, and 58 hydrogen bond distances. The ψ torsion angle restraints were all set to a range 50 ± 50° and ϕ values to either −120 ± 30° in extended structures or −60 ± 30° in α-helices; these mainly assist in the rate of convergence (Powers *et al.*, 1993). The H-bonding restraints were based on those H^N resonances remaining after 30 min at pH 6.75, 30 °C, and included 16 from the β-core and 42 from the helical regions; the N–O distance was constrained to 2.4–3.3 Å and the H–O value to 1.5–2.3 Å. The final 46 accepted SA structures have no NOE-derived distance violation greater than 0.5 Å and no torsion angle violation greater than 5°.

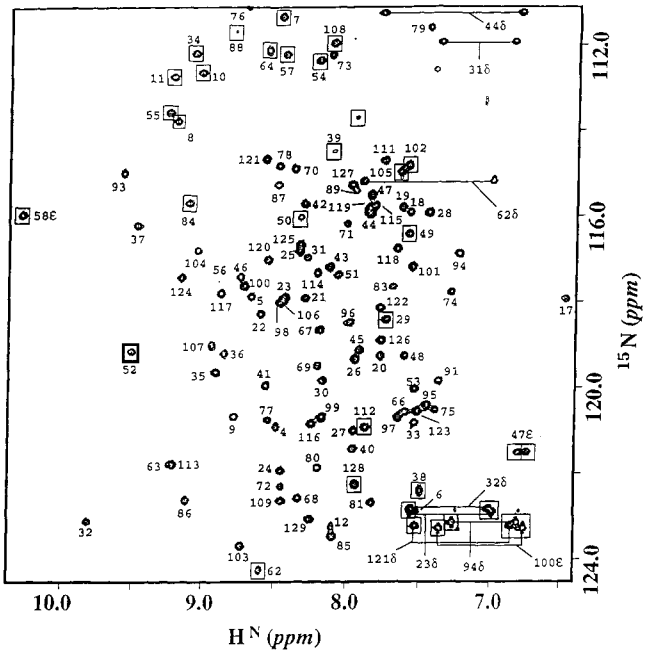

FIGURE 1: ^1H–^{15}N HSQC spectrum of *ca.* 2 mM uniformly ^{15}N-labeled CheY in the presence of 5 mM $MgCl_2$ at 30 °C, pH 6.75. An ^{15}N spectral width of 13.5 ppm was used to optimize the digital resolution. Aliased cross-peaks which are negative are shown surrounded by boxes. Assignments of isolated cross-peaks are indicated on the spectrum, and actual chemical shifts are listed in Table 1.

(3) Visualization of Three-Dimensional Structures. The structures were viewed by using either Insight II (BioSym Technologies) or ORIENT (G. T. Montelione) on a Silicon Graphics workstation. Atomic coordinates were superimposed using the algorithm of Kabsch (1978). The average rms deviations among a set of structures were calculated by determining the rms deviation between each pair of optimally superimposed structures in the set and then computing the average rms deviation; for these statistical analyses "backbone atoms" refer to N, C^α, and C′ atoms. The global fold of the protein was visualized using Insight II and the ribbon diagram constructed with the program Molscript (Kraulis, 1991).

RESULTS AND DISCUSSION

Spectra and Assignments. (1) ^1H, ^{15}N Correlation Spectra. A ^1H–^{15}N HSQC spectrum of uniformly ^{15}N-labeled CheY in the presence of 5 mM Mg^{2+} is shown in Figure 1. Since the HSQC spectrum forms the cornerstone of many of the ^{15}N-correlated or filtered experiments described herein, the figure shown maximizes the digital resolution by recording the ^{15}N dimension with reduced spectral width. Aliased cross-peaks, shown in boxes, are easily identified on the basis of their pure absorptive negative intensity in spectra recorded with a half dwell time initial delay (Bax *et al.*, 1991) and do not introduce additional overlap. This reduced spectral width was used for recording all 3D and 4D spectra involving ^{15}N, as well as the J-modulated HSQC, T_1, T_2, and heteronuclear NOE measurements. As expected in a well-defined protein structure, the spectrum is quite well dispersed but there are obvious regions of overlapping cross-peaks. This is not surprising since only 20% of the $(\beta/\alpha)_5$ structure is contained in β-strands (Volz, 1993) with the remainder distributed in

Table 1: ^{15}N, ^{13}C, and ^{1}H Resonance Assignments for CheY at pH 6.75 and 30 °C[a]

residue	N	C^{α}	C^{β}	others
A2		50.9 (3.90)	18.5 (0.81)	
D3		53.7 (4.49)	41.6 (2.73, 2.64)	
K4	120.8 (8.48)	57.0 (4.26)	30.5 (1.98, 1.77)	C^{γ} 24.5 (1.38, 1.27), C^{δ} 27.8 (1.19, 1.15), C^{ϵ} 42.0 (2.78)
E5	117.9 (8.68)	55.7 (4.48)	29.0 (2.27, 1.97)	C^{γ} 36.3 (2.35)
L6	122.7 (7.51)	56.4 (3.84)	43.1 (1.80, 1.63)	C^{γ} 26.2 (1.21), C^{δ} 25.0 (0.81), C^{δ} 26.5 (0.65)
K7	124.7 (8.47)	56.1 (5.10)	33.5 (1.88, 1.50)	C^{γ} (1.13), C^{δ} 29.1 (1.16, 0.83), C^{ϵ} 41.2 (2.47, 2.22)
F8	127.2 (9.20)	57.1 (5.41)	43.4 (3.21, 2.54)	C^{δ} 130.9 (7.02), C^{ϵ} 131.2 (6.21), C^{ζ} 128.0 (5.66)
L9	120.5 (8.78)	52.9 (5.13)	43.9 (1.70, 1.09)	C^{γ} (1.16), C^{δ} 22.7 (0.56), C^{δ} 27.1 (0.38)
V10	126.1 (9.04)	61.4 (4.80)	33.0 (1.99)	C^{γ} 21.1 (0.99)
V11	126.2 (9.21)	59.7 (4.82)	32.6 (2.27)	C^{γ} 21.4 (0.65), C^{γ} 21.3 (0.68)
D12	123.4 (8.11)	55.4 (4.65)	43.6 (2.74, 2.53)	
D13	122.9 (9.38)[b]	55.0 (5.08)	40.1 (2.98, 2.80)	
F14		54.3 (5.26)	38.1 (3.22)	C^{δ} 130.5 (7.42), C^{ϵ} 128.8 (7.36), C^{ζ} 128.5 (6.71)
S15				
T16		65.4 (3.77)	68.1 (3.23)	C^{γ} 21.5 (1.15)
M17	117.8 (6.49)	55.9 (4.51)	31.1 (2.18)	C^{γ} 32.6 (2.76, 2.66)
R18	115.8 (7.57)	60.5 (3.82)	30.5 (2.03, 1.81)	C^{γ} 24.3 (1.38, 1.28), C^{δ} 41.4 (2.92)
R19	115.6 (7.62)	58.8 (3.93)	29.4 (1.93)	C^{γ} 27.2 (1.70, 1.63), C^{δ} 43.1 (3.22, 3.05)
I20	119.0 (7.76)	65.4 (3.72)	37.8 (2.11)	C^{γ} 29.3 (1.80, 1.09), C^{δ} 13.2 (0.81), $C^{\gamma m}$ 16.3 (0.79)
V21	117.8 (8.28)	67.2 (3.43)	31.0 (2.15)	C^{γ} 23.4 (1.16), C^{γ} 22.6 (0.94)
R22	118.2 (8.60)	60.4 (3.82)	30.5 (2.03, 1.80)	C^{γ} 27.4 (1.52), C^{δ} 43.8 (3.27, 3.10)
N23	117.7 (8.42)	55.7 (4.56)	37.5 (3.03, 2.84)	N^{δ} 109.7 (7.53, 7.02)
L24	121.8 (8.44)	58.0 (4.16)	42.3 (2.06, 1.16)	C^{δ} 26.5 (0.73), C^{δ} 22.4 (0.87)
L25	116.6 (8.33)	58.2 (3.83)	40.1 (1.83, 1.34)	C^{γ} 26.5 (1.42), C^{δ} 26.7 (0.17), C^{δ} 22.3 (–0.14)
K26	119.2 (7.94)	59.8 (3.75)	31.6 (2.07)	C^{γ} 24.7 (1.63, 1.41), C^{δ} 29.6 (1.79), C^{ϵ} 41.4 (2.98)
E27	120.9 (7.95)	59.3 (3.99)	28.8 (2.3, 2.17)	C^{γ} 36.0 (2.45)
L28	115.7 (7.43)	54.3 (4.28)	42.2 (2.16, 1.83)	C^{γ} 26.1, C^{δ} 24.8 (0.88), C^{δ} 21.8 (0.88)
G29	104.9 (7.74)	44.6 (3.94, 3.54)		
F30	119.7 (8.17)	57.1 (4.86)	38.6 (3.08, 2.45)	C^{δ} 132.9 (7.29), C^{ϵ} 130.8 (7.31)
N31	116.8 (8.28)	53.6 (4.68)	40.5 (2.83, 2.66)	N^{δ} 111.8 (7.39, 6.88)
N32	123.0 (9.82)	52.1 (5.01)	36.4 (3.27, 2.88)	N^{δ} 109.2 (7.56, 7.00)
V33	120.8 (7.53)	60.8 (4.99)	36.3 (1.85)	C^{γ} 22.6 (0.83)
E34	125.4 (9.06)	53.8 (4.93)	34.0 (2.31, 2.16)	C^{γ} 36.2 (2.57, 2.45)
E35	119.6 (8.92)	54.7 (5.44)	34.8 (1.90)	C^{γ} 35.5 (2.15, 2.06)
A36	119.0 (8.84)	50.1 (4.81)	22.7 (1.30)	
E37	116.1 (9.48)	56.7 (4.62)	31.8 (2.06)	C^{γ} 35.7 (2.20)
D38	108.9 (7.49)	53.7 (5.30)	41.3 (3.51, 3.30)	
G39	100.8 (8.08)	48.4 (3.75, 3.61)		
V40	121.4 (7.95)	65.9 (3.50)	31.4 (2.26)	C^{γ} 21.1 (0.90)
D41	119.8 (8.57)	56.4 (4.44)	42.4 (2.97, 2.60)	
A42	115.6 (8.30)	55.0 (3.61)	19.8 (1.36)	
L43	117.1 (8.12)	58.2 (3.75)	41.2 (1.74, 1.51)	
N44	115.6 (7.85)	56.0 (4.39)	38.0 (3.05, 2.88)	N^{δ} 111.1 (7.78, 6.83)
K45	119.0 (7.92)	60.0 (4.11)	31.9 (1.76)	C^{γ} 24.5 (1.43), C^{δ} 29.0 (1.69), C^{ϵ} 41.7 (2.96)
L46	117.3 (8.75)	57.2 (3.83)	42.1 (1.75, 1.41)	C^{δ} 25.3 (0.53), C^{δ} 22.6 (0.36)
Q47	115.3 (7.84)	57.7 (4.03)	28.1 (2.15)	C^{γ} 33.8 (2.56), N^{γ} 107.9 (6.83, 6.78)
A48	119.1 (7.60)	53.3 (4.31)	19.0 (1.67)	
G49	102.7 (7.58)	44.5 (4.31, 4.08)		
G50	102.5 (8.34)	45.2 (3.94, 3.67)		
Y51	117.2 (8.07)	60.6 (4.07)	39.0 (3.05, 2.53)	C^{δ} 133.0 (6.93), C^{ϵ} 117.9 (6.69)
G52	105.7 (9.53)	44.3 (4.51, 3.44)		
F53	120.1 (7.55)	58.0 (4.10)	43.4 (2.01)	C^{δ} 132.0 (6.89), C^{ϵ} 130.0 (6.87), C^{ζ} 128.4 (6.79)
V54	125.6 (8.21)	61.1 (5.13)	34.6 (2.09)	C^{γ} 22.3 (0.83), C^{γ} 20.6 (0.74)
I55	126.7 (9.23)	60.4 (5.10)	40.1 (1.87)	C^{γ} 27.8 (2.01, 1.21), C^{δ} 14.0 (0.77) $C^{\gamma m}$ 17.7 (0.91)
S56	117.4 (8.93)	56.2 (5.40)	65.8 (3.64, 3.06)	
D57	125.4 (8.44)	54.5 (5.10)	38.7 (3.26, 2.92)	
W58		59.8 (4.21)	30.6 (3.60, 3.51)	$C^{\delta 2}$ 126.6 (7.27), $C^{\epsilon 3}$ 118.5 (7.42), $C^{\zeta 2}$ 114.7 (7.47), $C^{\zeta 3}$ 120.0 (6.79), C^{η} 124.2 (7.28), $N^{\epsilon 1}$ 129.4 (10.3)
N59	115.0 (8.14)[b]	54.7 (5.12)	(2.86)	
M60	122.5 (7.36)[b]	53.8 (4.80)	34.3 (2.20, 2.07)	
P61		62.1 (4.42)	32.7 (1.94)	C^{γ} 26.8 (2.14), C^{δ} 50.2 (3.80, 3.64)
N62	110.6 (8.62)	59.0 (4.05)	37.5 (3.28, 2.65)	N^{δ} 115.1 (7.91, 7.02)
M63	121.7 (9.27)	56.9 (4.21)	35.5 (2.19)	31.0 (2.41)
D64	125.8 (8.60)	53.0 (4.49)	40.5 (3.72, 2.92)	
G65	102.1 (8.63)[b]	47.2 (3.99, 3.48)		
L66	120.5 (7.56)	56.9 (3.74)	40.5 (1.49, 0.86)	C^{γ} 26.8 (1.16), C^{δ} 24.3 (0.73)
E67	118.5 (8.19)	58.9 (3.84)	28.9 (1.97, 1.86)	C^{γ} 36.0 (2.31)
L68	122.4 (8.32)	58.6 (4.09)	41.0 (2.07, 1.15)	C^{γ} 26.7 (1.35), C^{δ} 25.9 (0.78), C^{δ} 22.4 (0.90)
L69	119.4 (8.20)	58.3 (3.78)	41.0 (2.11, 1.60)	C^{δ} 27.5 (0.83), C^{δ} 22.2 (0.65)
K70	114.7 (8.36)	59.8 (3.80)	32.0 (1.86, 1.77)	C^{γ} 24.5 (1.41), C^{δ} 29.0 (1.67), C^{ϵ} 41.7 (2.96)
T71	116.0 (8.00)	67.1 (3.81)	68.1 (4.35)	C^{γ} 22.2 (1.20)
I72	122.2 (8.45)	65.7 (3.39)	38.6 (1.88)	C^{γ} 29.3 (1.68, 0.81), C^{δ} 14.5 (0.56), $C^{\gamma m}$ 17.1 (0.74)
R73	112.0 (8.12)	57.0 (4.01)	29.0 (1.98, 1.64)	
A74	117.6 (7.28)	51.7 (4.34)	19.1 (1.42)	
D75	120.4 (7.40)	53.8 (4.58)	43.8 (2.90, 2.60)	
G76	111.1 (8.74)	47.2 (3.90)		
A77	120.5 (8.57)	53.3 (4.50)	19.4 (1.49)	

Table 1: (Continued)

residue	N	C^{α}	C^{β}	others
M78	114.7 (8.48)	55.8 (4.59)	34.2 (2.23, 2.13)	C^{γ} 34.0 (2.62, 2.39)
S79	111.3 (7.45)	61.8 (4.38)	63.3 (4.07, 3.98)	
A80	121.8 (8.20)	50.9 (4.45)	18.7 (1.33)	
L81	122.6 (7.83)	53.6 (4.16)	42.8 (1.54, 1.29)	C^{γ} 26.5 (1.54), C^{δ} 25.0 (0.71)
P82		62.3 (4.01)	31.4 (1.39, 0.42)	C^{γ} 27.8 (1.86, 1.68), C^{δ} 51.1 (3.88, 3.56)
V83	117.5 (7.68)	60.2 (4.79)	35.9 (1.68)	C^{γ} 20.5 (0.68)
L84	129.0 (9.10)	52.5 (4.55)	45.4 (2.11, 1.15)	C^{γ} 26.7 (1.31), C^{δ} 25.8 (0.51)
M85	123.4 (8.09)	52.7 (5.53)	31.9 (2.14, 2.06)	C^{γ} 31.9 (2.45)
V86	122.4 (9.11)	60.9 (4.99)	33.0 (2.14)	C^{γ} 22.7 (1.11), C^{γ} 20.3 (0.82)
T87	115.2 (8.50)	58.6 (5.10)	70.4 (4.07)	C^{γ} 19.4 (0.92)
A88	124.8 (8.81)	52.5 (4.63)	19.7 (1.53)	
E89	115.3 (7.97)	56.0 (4.32)	29.2 (1.90)	C^{γ} 2.10
A90		51.3 (4.21)	17.4 (1.28)	
K91	119.8 (7.38)	55.1 (4.40)	33.0 (1.78, 1.55)	C^{γ} 24.8 (1.30), C^{δ} 28.9 (1.60), C^{ϵ} 41.7 (2.90)
K92		59.8 (3.76)	31.9 (1.87, 1.77)	C^{γ} 24.5 (1.40), C^{δ} 29.0 (1.66), C^{ϵ} 41.8 (2.92)
E93	114.9 (9.59)	59.8 (3.95)	28.5 (1.93)	C^{γ} 36.3 (2.27)
N94	116.7 (7.23)	54.7 (4.56)	36.9 (2.56, 2.05)	N^{δ} 109.4 (7.30, 6.85)
I95	120.3 (7.44)	64.8 (3.17)	37.3 (1.67)	C^{γ} 27.8 (1.00, 0.26), C^{δ} 12.3 (0.38), $C^{\gamma m}$ 16.7 (0.55)
I96	118.3 (7.96)	64.3 (3.79)	37.6 (1.67)	C^{γ} 28.6 (1.59, 1.17), C^{δ} 12.8 (0.81), $C^{\gamma m}$ 16.8 (0.90)
A97	120.5 (7.64)	55.0 (4.21)	18.1 (1.72)	
A98	117.9 (8.46)	54.8 (3.92)	16.9 (1.53)	
A99	120.5 (8.16)	55.3 (4.21)	17.7 (1.59)	
Q100	117.5 (8.70)	58.5 (4.04)	28.1 (2.19, 2.10)	C^{γ} 34.2 (2.63, 2.44), N^{γ} 109.8 (7.36, 6.77)
A101	117.0 (7.56)	51.7 (4.35)	19.1 (1.43)	
G102	101.1 (7.59)	45.6 (4.22, 3.89)		
A103	123.6 (8.72)	53.5 (3.94)	18.4 (1.37)	
S104	116.6 (9.04)	60.0 (4.42)	61.0 (3.98, 3.27)	
G105	101.3 (7.64)	44.7 (4.14, 3.85)		
Y106	117.9 (8.44)	56.0 (5.88)	41.3 (2.81)	C^{δ} 133.0 (6.78), C^{ϵ} 117.3 (6.60)
V107	118.9 (8.95)	59.4 (4.29)	35.2 (1.49)	C^{γ} 21.6 (0.48), C^{γ} 20.6 (0.40)
V108	125.1 (8.11)	60.4 (4.99)	36.3 (1.86)	C^{γ} 22.6 (0.82)
K109	122.5 (8.45)	53.4 (4.64)	32.9 (1.72)	C^{γ} 24.4 (1.33), C^{δ} 29.4 (1.62), C^{ϵ} 41.2 (2.93)
P110		62.2 (4.39)	34.4 (2.27, 1.99)	C^{γ} 24.4 (1.93), C^{δ} 50.0 (3.67, 3.48)
F111	114.5 (7.75)	53.6 (5.50)	40.6 (3.39, 2.99)	C^{δ} 133.0 (7.09), C^{ϵ} 130.3 (7.08), C^{ζ} 127.9 (7.00)
T112	107.3 (7.86)	59.3 (4.54)	71.7 (4.80)	C^{γ} 21.6 (1.34)
A113	121.7 (9.20)	55.8 (3.97)	17.1 (1.50)	
A114	117.1 (8.21)	54.9 (4.25)	18.0 (1.47)	
T115	115.5 (7.81)	65.8 (4.06)	68.3 (4.30)	C^{γ} 22.3 (1.22)
L116	120.7 (8.24)	58.1 (3.65)	40.9 (2.07, 1.43)	C^{γ} 26.7 (1.33), C^{δ} (0.74), C^{δ} 21.2 (0.45)
E117	117.7 (8.89)	59.9 (3.64)	29.6 (2.25)	C^{γ} 35.5 (2.41, 2.21)
E118	116.6 (7.66)	59.4 (4.07)	29.3 (2.20)	C^{γ} 36.0 (2.46)
K119	115.6 (7.84)	57.5 (3.95)	31.5 (1.92, 1.42)	C^{γ} 24.5 (1.09), C^{δ} 27.5 (1.61), C^{ϵ} 41.6 (2.87)
L120	116.8 (8.55)	57.8 (3.41)	40.4 (1.64, 0.83)	C^{γ} 26.1 (1.45), C^{δ} 25.7 (0.38), C^{δ} (0.08)
N121	114.5 (8.58)	56.0 (4.56)	37.3 (3.03, 2.86)	N^{δ} 110.1 (7.53, 6.86)
K122	117.9 (7.78)	58.7 (4.15)	32.0 (1.95)	C^{γ} 25.1, C^{δ} 28.3 (1.60), C^{ϵ} 41.8 (2.97)
I123	120.5 (7.51)	65.4 (3.73)	37.7 (1.89)	C^{γ} 29.8 (1.87, 0.86), C^{δ} 15.2 (0.68), $C^{\gamma m}$ 17.8 (0.91)
F124	117.3 (9.14)	58.7 (4.67)	37.2 (3.48, 3.33)	C^{δ} 130.8 (7.48), C^{ϵ} 130.8 (7.26), C^{ζ} 128.4 (6.69)
E125	116.5 (8.32)	59.2 (4.24)	29.8 (2.27, 2.20)	C^{γ} 36.0 (2.46)
K126	118.7 (7.75)	58.4 (4.18)	32.2 (2.07, 1.91)	C^{γ} 25.0 (1.65), C^{δ} 28.6 (1.74), C^{ϵ} 41.8 (3.03)
L127	115.1 (7.96)	54.6 (4.42)	42.5 (1.83, 1.76)	C^{γ} 27.0 (1.93), C^{δ} 22.0 (0.93)
G128	108.8 (7.97)	46.5 (4.01)		
M129	123.1 (8.25)	57.0 (4.21)	35.5 (2.18, 1.85)	C^{γ} 32.4 (2.60, 2.44)

[a] In each column, ^{15}N and ^{13}C chemical shifts are listed first, and the corresponding ^{1}H chemical shifts are in parentheses. ^{1}H and ^{13}C values are relative to external TSP at pH 6.5, 30 °C. ^{15}N values are relative to external anhydrous $^{15}NH_3$ at 25 °C; 117.8 ppm is the chemical shift of an absolute frequency of 60.792293 at a field where TSP occurs at 599.877371 MHz. [b] Observed in ^{15}N-enriched Gly, Met, or Asx CheY samples.

α-helices (40%), loops bracketing the repetitive secondary structure (25%), and other loops (15%). The spectrum is different in the absence of Mg^{2+} with distinguishable chemical shift changes occurring in the metal binding region. Recent estimates (Lukat *et al.*, 1990) of the $K_d \sim 0.5$ mM for the CheY–Mg^{2+} complex imply approximately 90% of the protein is in the Mg^{2+}-bound form under these conditions. Higher concentrations of Mg^{2+} (30 mM) are required to observe additional correlations because of chemical exchange between the apoprotein and the Mg^{2+} form, *vide infra*.

At a later stage, as part of the study of phosphorylation, we also recorded ^{1}H-^{15}N HSQC spectra of samples with specifically ^{15}N-enriched amino acids (Gly, Leu, Lys, Asx, Val, Met), but earlier in the assignment process a sample of [^{15}N]Ala was available and provided a convenient starting point for sequential assignment because of the unique string of A97-A98-A99 in the primary sequence. During the assignment process these spectra of the specifically labeled amino acids provided convenient checks of the spin type but were not used extensively in making the sequential assignment.

(2) ^{1}H, ^{13}C, and ^{15}N Resonance Assignments. The backbone sequential assignments were determined from the 4D HNNCAHA (Boucher *et al.*, 1992a; Kay *et al.*, 1992; Olejniczak *et al.*, 1992; Clubb *et al.*, 1992) and 4D HCA(CO)NNH (Boucher *et al.*, 1992b) spectra, but because of overlap in regions of the C^{α} and H^{α} plane for some helical regions of the protein, the 3D HCCH COSY and 3D HCCH TOCSY spectra were required to unequivocally identify the amino acid type during the process. With current methodology this overlap problem is more conveniently resolved with the 4D TOCSY-HCC(CO)NNH triple-resonance experiment, in place of the 4D HCA(CO)NNH and 3D HCCH TOCSY

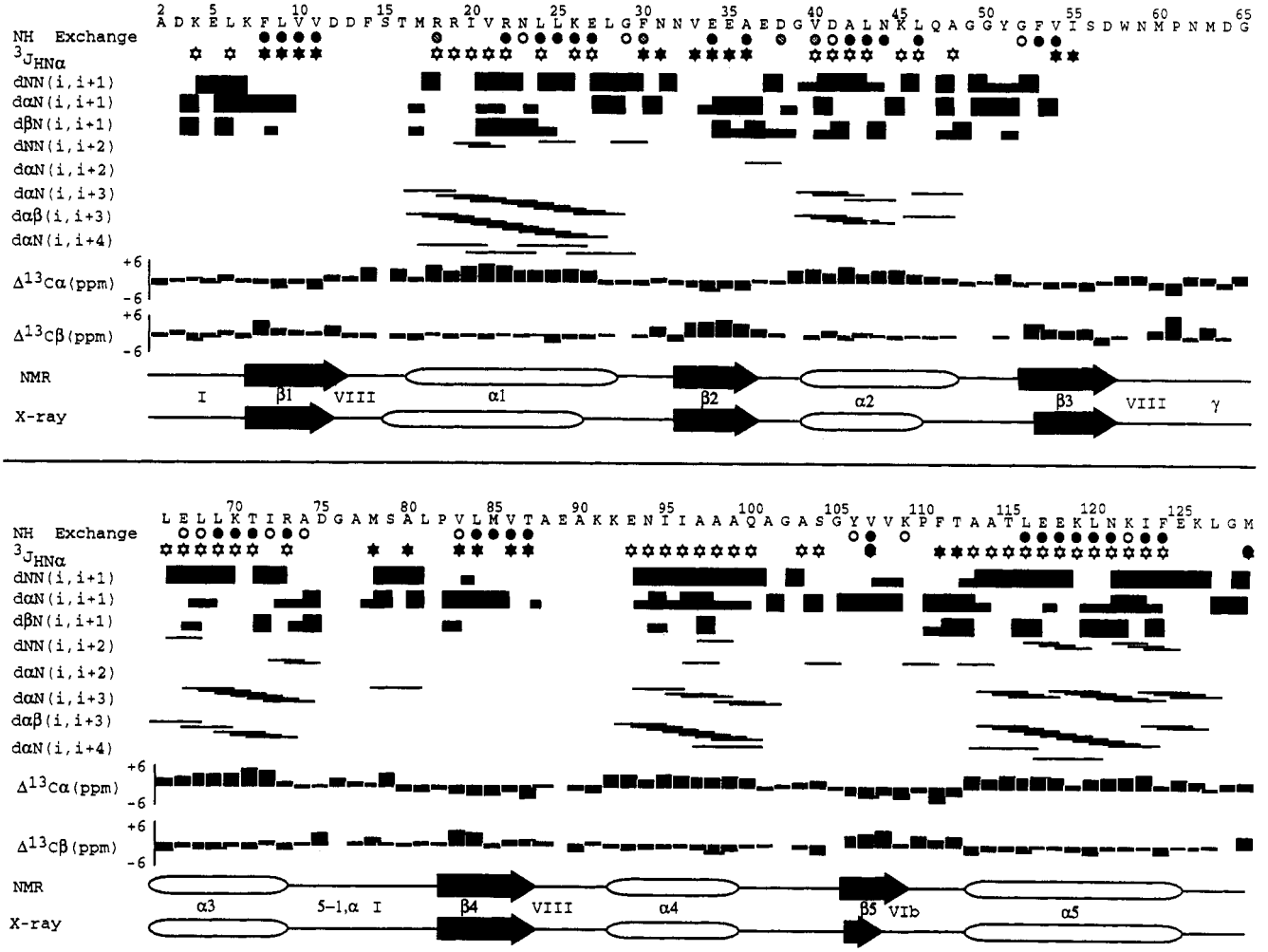

FIGURE 2: Diagram of the sequential and medium-range NOE connectivities, labile hydrogen exchange rates, three-bond $^3J_{HnH\alpha}$ coupling constants, and variation of $^{13}C^{\alpha}$ and $^{13}C^{\beta}$ chemical shifts from random coil values for CheY. The NOE correlations were determined from the 3D ^{15}N- and ^{13}C-edited NOESY-HMQC, 3D ^1H–^{15}N HMQC-NOESY-HMQC, 4D $^{13}C/^{15}N$-edited NOESY, and $^{13}C/^{13}C$-edited NOESY spectra at 30 °C and pH 6.75. The height of the bars reflects the strength of the NOE correlation as strong, medium, or weak. Filled circles represent H^N nuclei that are still present after 38 min at pH 6.75, 30 °C, while open circles are nuclei detectable after 22 min; only residues remaining 38 min were considered for assignment as a hydrogen bond acceptor in the structure calculation. Small (<5 Hz) and large (>8 Hz) $^3J_{HnH\alpha}$ coupling constants are indicated by open and filled stars, respectively. Deviations of ^{13}C shifts from random coil values are self-explanatory.

experiment (Richardson *et al.*, 1993; Lyons & Montelione, 1993; Grzesiek *et al.*, 1993; Logan *et al.*, 1993), but at the time of data analysis these experiments were not available, nor indeed needed, to confidently assign CheY.

Unique spins systems (Ala, Gly, Val, Thr, Leu, Ile, and Lys) determined from the 3D HCCH-COSY, 3D HCCH-TOCSY, and 3D ^{15}N-edited HOHAHA served as useful starting points in the sequential assignments, as well as the [^{15}N]Ala described above. The sequential resonance assignments based solely on these scalar coupling experiments are determined for the strings of residues from Asp-3 to Asp-12, Thr-16 to Asp-57, Pro-61 to Asp-64, Gly-65 to Leu-81, Pro-82 to Glu-89, Ala-90 to Lys-91, Lys-92 to Lys-109, and Pro-110 to Met-129. Incomplete H^N assignments at this stage, Ala-2, Asp-3, Asp-13 to Thr-16, Trp-58 to Met-60, Gly-65, Ala-90, and Lys-92, all occur either at, or proximal to, loop regions. These backbone amide resonances are weakened in intensity by saturation transfer (Moy *et al.*, 1992) and/or intramolecular dynamical effects. The H^{α}, C^{α}, H^{β}, and C^{β} of Ala-2 were assigned in the HCCH-COSY and -TOCSY on the basis of its unique spin system, and subsequently verified on a $^{13}C^{\beta}$ specifically labeled alanine CheY sample (data not shown). The H^N and ^{15}N of Asp-13, Asn-59, and Met-60 were identified later in 2D ^1H–^{15}N HSQC and 2D ^{15}N HMQC TOCSY spectra acquired on specifically ^{15}N-labeled Asx or Met CheY samples containing 30 mM $MgCl_2$; the higher Mg^{2+} slows the NH exchange. The amide ^1H and ^{15}N of Gly-65 was determined from an unassigned peak in the ^1H–^{15}N HSQC spectrum on a specifically labeled [^{15}N]Gly CheY sample. The H^{α} were assigned on the basis of a 2D ^{15}N HMQC TOCSY and then connected with the characteristic C^{α} chemical shift from the 2D ^{13}C-HSQC. Although sequential connections to Pro-61 were not identified, the only remaining characteristic proline C^{δ}, H^{δ} was assigned in the 2D ^{13}C-HSQC and connected with the side-chain atoms in the 3D HCCH-TOCSY. All aromatic side-chains were assigned by making connections to their intraresidue H^{α}, C^{α} and H^{β}, C^{β} from the 3D ^{13}C-edited NOESY; the H^N, ^{15}N of Phe-14 and Trp-58 have not been assigned most likely because of Mg^{2+} exchange broadening. Other remaining unassigned H^N, ^{15}N are Ser-15, Thr-16, Ala-90, and Lys-92, all of which are in close proximity to the Mg^{2+} binding site and situated in loops. Lys-92 C^{α} and H^{α} chemical shifts were tentatively assigned on the basis of a medium NOE from Ile-95 H^{β} to an unassigned C^{α} and H^{α} chemical shift using the 3D NMR structure which indicated that Lys-92 to Ile-95 is in a helical region; these assignments were later validated using other scalar coupling experiments. These less certain structure-based assignments

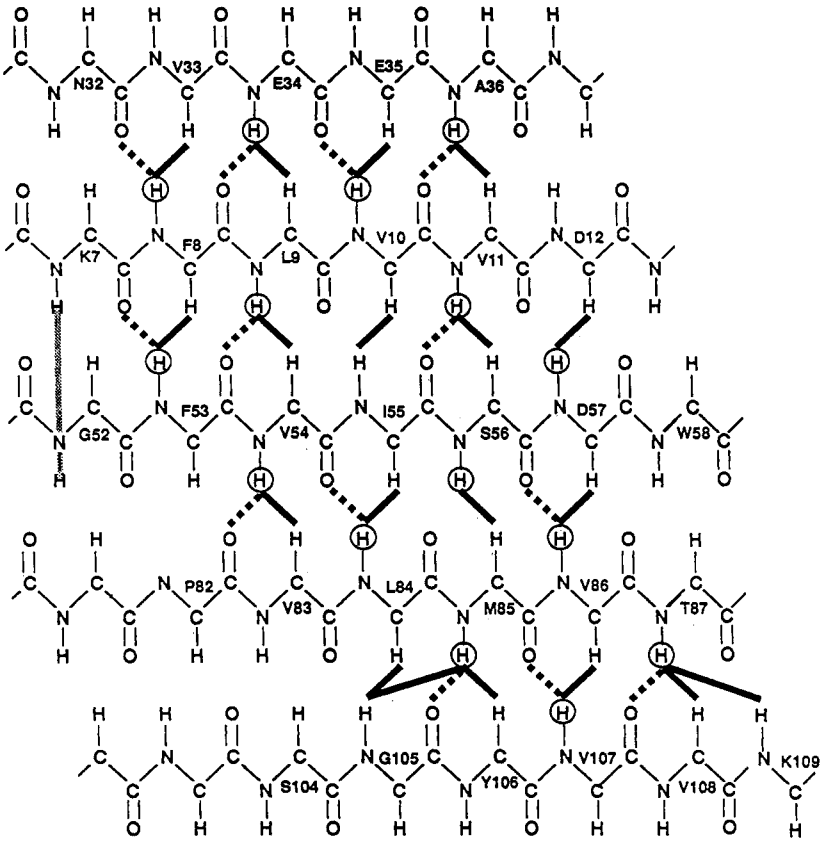

FIGURE 3: Intrastrand NOE contacts observed in the 5-stranded parallel β-sheet of the core of CheY and the hydrogen-bonding donor–acceptor pairs in the same region. NOE's are depicted as solid lines (or stippled for H^N–H^N) while hydrogen-bonded pairs are shown as dashes. Backbone–side-chain NOE's are also observed between residues K7 and N32, F53 and P82, and V83 and S104.

were only included at a later stage to minimize the possibility of errors. The cumulative ^1H, ^{13}C, and ^{15}N assignments are listed in Table 1.

Identification of Secondary Structure. (1) Sequential and Medium-Range Assignments from NOESY Spectra. As part of gathering the structural restraints the sequential assignments were validated independently of the 4D HNNCAHA and 4D HCA(CO)NNH spectra by using the 3D ^{15}N- and ^{13}C-edited NOESY, 3D ^1H–^{15}N HMQC-NOESY-HMQC, 4D $^{13}C/^{15}N$-edited NOESY, and 4D $^{13}C/^{13}C$-edited NOESY spectra. The ^{15}N-edited NOESY spectra provide the sequential dNN(i,i+1), dαN(i,i+1), dβN(i,i+1) NOE's and the medium-range dαN(i,i+2), dNN(i,i+2), dαN(i,i+3), and dαN(i,i+4) NOE's. The 3D ^1H–^{15}N HMQC-NOESY-HMQC spectrum proves useful in α-helices, where sequential H^N–H^{N+1} are oftentimes degenerate, by transferring the chemical shift information to $^{15}N_i$–$^{15}N_{i+1}$. Residues which fall into this category, with sequential H^N–H^{N+1} chemical shift differences $\leq$0.05 ppm, include Arg-18/Arg-19, Asn-23/Leu-24, Lys-26/Glu-27, Ala-48/Gly-49, Ala-101/Gly-102, Leu-120/Asn-121, and Leu-127/Gly-128. The d$\alpha\beta$(i,i+3) NOE's found in helical regions (Wüthrich, 1986) are clearly identified in the 3D ^{13}C-edited NOESY.

The upper portion of Figure 2 diagrams the short- and medium-range NOE's which are illustrative of secondary structure elements. A noteworthy observation is that the sequential discontinuities observed in the 4D HNNCAHA and 4D HCA(CO)NNH experiments are also mirrored in the 3D and 4D NOESY experiments, involving H^N. Five helical segments are identified approximately between residues 16–28, 39–48, 65–73, 92–99, and 113–125 and five (parallel) β-strands between 7–12, 32–36, 52–57, 82–87, and 105–109.

(2) ^{13}C Chemical Shifts. In addition to short- and medium-range NOE's, the deviation of ^{13}C chemical shifts from random coil values provides direct evidence of secondary structure (Spera & Bax, 1991). Since these values are immediately available from our heteronuclear assignments, Figure 2 includes these variations of both C^α and C^β shifts and clearly shows similar regions of regular secondary structure. A noteworthy ^{13}C shift is the low-field position of the C^β of Pro-110 which is diagnostic of a cis-peptide bond (Shirakawa *et al.*, 1993; Kraulis *et al.*, 1994) and borne out by the characteristic NOE between Lys-109 (H^α) and Pro-110 (H^α). There is no indication of an NOE between Lys-109 (H^α) and Pro-110 (H^δ) which would be characteristic of a trans-peptide bond or cis/trans isomerism.

(3) $^3J(H^N$–$H^\alpha)$ Coupling Constants. A large number of $^3J(H^N$–$H^\alpha)$ coupling constants, which determine the torsion angle ϕ, have been measured by two methods; a pseudo 3D J-modulated ^{15}N–^1H correlation experiment on ^{15}N-labeled CheY and a 3D coupled HNCA experiment, which correlates H^N, ^{15}N, $^{13}C^\alpha$, on (^{13}C, ^{15}N)-labeled CheY. These measurements were used semiquantitatively to assess secondary structure; the precision of the J-modulated HSQC for smaller J values is limited by the dominance of the short T_2' (Billeter *et al.*, 1992) while differential relaxation limits the accuracy of the HNCA experiment (Gorlach *et al.*, 1993). A very recent paper (Vuister & Bax, 1993) provides an alternative experiment to more easily and accurately quantitate these couplings but was not available at the time of our data collection. Nevertheless, twenty $^3J(H^N$–$H^\alpha)$ coupling constants $\geq$8 Hz were measured and attributed to the extended structure found in β-strands or loops; accordingly, the backbone torsion angle ϕ was restrained to $-120 \pm 30°$ for structure calculations. The apparent transverse relaxation time T_2' is

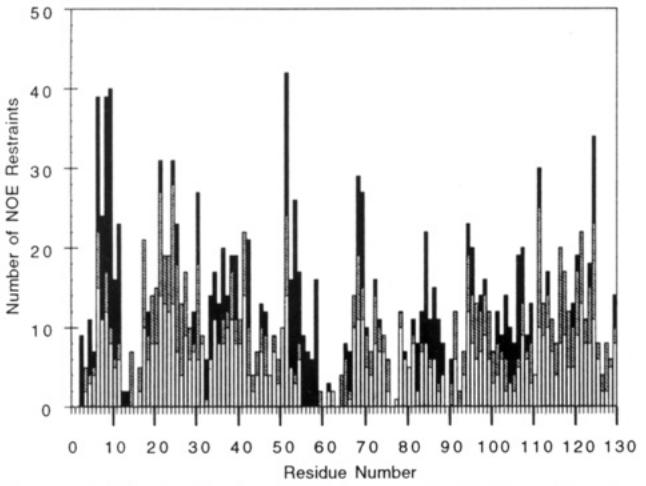

FIGURE 4: The distribution of NOE contacts in CheY as a function of sequence position. Short-, medium-, and long-range interactions are shown separately as open, cross-hatched, and filled boxes, respectively Several regions of the protein (D13 to T16, W58 to N63, and A88 to K91) have relatively few NOE's because of exchange broadening.

also determined from the pseudo 3D J-modulated ^{15}N–^{1}H correlation experiment and shows values of *ca.* 30 ms in the β-strands and *ca.* 40 ms in the loops; α-helices are intermediate with T_2' values of 35 ms. However, these differential dynamics are better supported by genuine relaxation data presented later. Forty-eight residues had $^{3}J(H^N–H^\alpha)$ coupling constants $\leq$5 Hz indicative of α-helical structure so the ϕ torsion angle was restrained to $-60 \pm 30°$ in structure calculations. The combined measurements of $^{3}J(H^N–H^\alpha)$ are shown in Figure 2; wherever values were determined from both experiments, the constant determined from the J-modulated HSQC is shown. Once ϕ torsion angles and NOE values confirmed helical secondary structure, we also examined the $^{13}C^\alpha$ chemical shifts for their characteristic downfield shifts (Spera & Bax, 1991). When all three parameters were mutually internally consistent, the corresponding ψ torsion angle restraints were all set to a range $50 \pm 50°$.

(4) Hydrogen/Deuterium Exchange. The sequence positions of slow and intermediate exchange rates for H^N are also included in Figure 2. Strips of slowly exchanging amides are observed from Phe-8 to Val-11, Phe-53 to Val-54, and Leu-84 to Thr-87, comprising the central core three strands of the five-stranded parallel β-sheet. Alternating fast and slow exchange is observed at Glu-34 (slow), Glu-35 (fast), and Ala-36 (slow), demonstrating that this β_2-strand is on the outer extreme of the sheet. The β_5 strand expected at the other side of the sheet, although longer by other NMR indicators, does not show definitive alternation although there are hints with slower exchange observed for Val-107 and Lys-109. Figure 3 shows the slowly exchanging amides along with the NOE's observed between the β-strands, and forming the core of the tertiary structure. Approximate helical regions are indicated between residues 15–30, 40–46, 65–73, and 113–124. No slowly exchanging amides were observed in the α_4-helix from 92 to 99 which lies in close proximity to the region of phosphorylation.

Calculation of the Global Fold. The identification of short- and medium-range NOE cross-peaks shows that CheY is composed of extensive regular secondary structure. However, the distribution of short-, medium- and long-range NOE contacts depicted in Figure 4 shows regions of the protein which are deficient in NOE's suitable to accurately define the tertiary structure. Therefore, in the absence of a more thorough analysis of additional NOE's obtained in samples with higher Mg^{2+} concentration, our structure calculations are restricted to determining the global fold of the protein. Moreover, the recent 1.8-Å resolution crystal structures of *Salmonella typhimurium* CheY with and without Mg^{2+} (Stock *et al.*, 1993) obviate a more detailed structure.

FIGURE 5: Overlay of 10 of the 46 converged SA conformers of CheY. Structures are shown with optimal overlap of the backbone atoms from the five α-helices and β-core residues in Table 2.

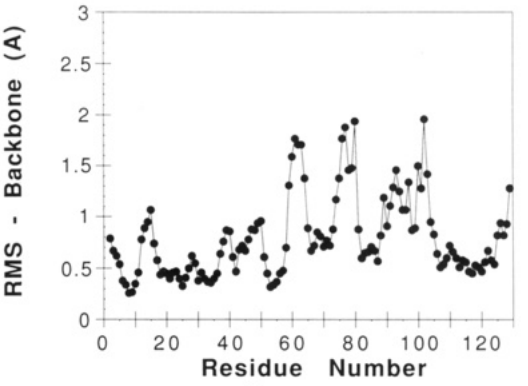

FIGURE 6: The rms deviation (Å) of the backbone C′, C^α, and N atoms for the ensemble of 46 SA structures of CheY.

Table 2: Comparison of the 46 SA Structures of CheY Used To Represent the Solution Structure

CheY segment	mean rms deviation (Å)	
	backbone atoms	heavy atoms
2–129	1.34 (0.24)[a]	2.02 (0.20)
2–58, 65–129	1.26 (0.25)	1.88 (0.20)
helix I (15–26)	0.43 (0.13)	1.61 (0.32)
helix II (39–46)	0.32 (0.13)	0.97 (0.17)
helix III (65–73)	0.46 (0.12)	1.42 (0.26)
helix IV (92–99)	0.54 (0.17)	1.39 (0.24)
helix V (113–125)	0.39 (0.10)	1.31 (0.17)
β core[b]	0.52 (0.15)	1.18 (0.15)
helices and β core[c]	0.98 (0.23)	1.65 (0.18)
av rms difference to the mean structure	0.95	1.43
rms difference to av vs X-ray	1.27	1.84

[a] The standard deviations are in parentheses. [b] The β core includes residues 7–11, 32–36, 53–57, 82–87, and 106–109. [c] The helices and β core defined here are composed of 75 residues.

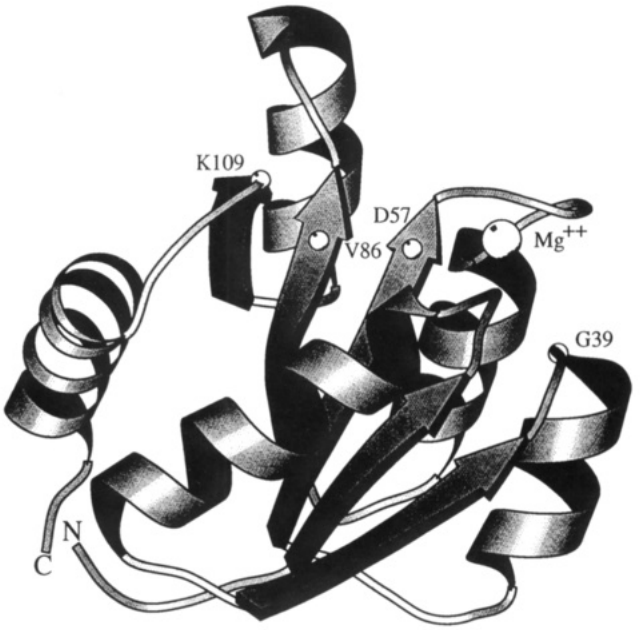

FIGURE 7: Ribbon diagram depiction (Molscript; Kraulis, 1991) of one of the 46 converged simulated annealing structures of CheY. This view is similar to that of the most recent X-ray structure (Stock *et al.*, 1993) and clearly shows the 5-stranded parallel β-sheet with 3 helices on one side and 2 helices on the other. We do not locate the position of the Mg^{2+} in our structure calculation, so the rendition is based on the position inferred from the X-ray structure.

The 46 converged simulated annealing (SA) structures, starting from 60 subembedded structures, were calculated with 1032 experimental NMR restraints. The rms deviation of the backbone atoms N, C^{α}, and C' for residues 2–129 is 1.34 Å, and the rms deviation to the mean is 0.95 Å. The 852 approximate interproton distance restraints were classified as follows: 158 intraresidue, 214 sequential interresidue ($|i-j| = 1$), 228 medium-range ($1 < |i-j| \leq 5$), and 252 long-range ($|i-j| > 5$). Also included in the final structure calculations were 44 ψ torsion angles which were identified in helical regions, 68 ϕ torsion angles from $^3J(H^N-H^{\alpha})$, and 58 hydrogen bond distances. The quality of the structure is depicted in a backbone trace of 10 representative conformers from the 46 final converged SA calculations shown in Figure 5 and in the backbone atom rms deviation shown in Figure 6. Not surprisingly the backbone deviation mirrors the number of NOE restraints per residue shown in Figure 4. Particularly noteworthy are the large deviations in the regions of residues 15–16, 61–66, 75–79, and 91–102 which are seriously lacking in long-range constraints. The statistics obtained from the ensemble of 46 structures used to represent the structure are shown in Table 2. A ribbon diagram (Kraulis, 1991) of the calculated structures showing a similar perspective to the ensemble is shown in Figure 7.

^{15}N Relaxation and Protein Dynamics. Several times throughout this paper we have alluded to amide protons which were not observed in ^{15}N–$^1H^N$ correlation spectra because of

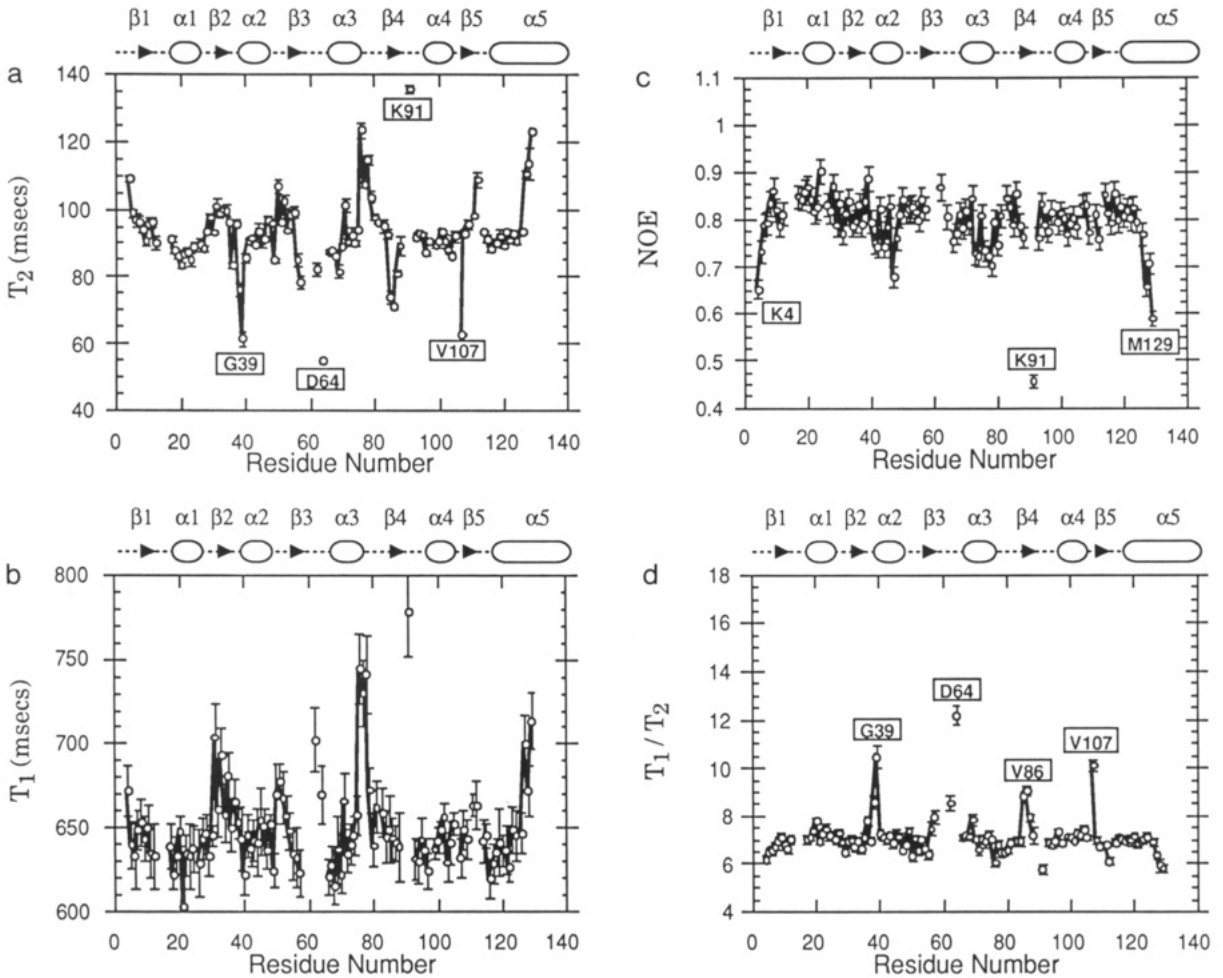

FIGURE 8: Plots of relaxation parameters for the backbone amide ^{15}N nuclei as a function of sequence position. 106 out of a possible 128 values are shown; gaps occur in the sequence for D13, N59, M60, and G65 because they are only observed at higher Mg^{2+} concentration and for A2, D3, F14, S15, T16, W58, A90, and K92 because they are not observed at all. Cross-peak overlap precludes measurement of L25, M63, E89, A98, Y106, A113, and E125. The three prolines at positions 61, 82, and 110 are not detected in these experiments. (a) T_2; (b) T_1; (c) heteronuclear NOE; (d) T_1/T_2.

chemical exchange. These exchange-broadened resonances are observed, however, at higher Mg^{2+} concentration where the dominant species is the Mg^{2+}-bound form; at lower concentration broadening occurs because the rate of the exchange process is approximately the same as the chemical shift differences between the free and Mg^{2+}-bound forms, both of which are at appreciable concentration because of the small K_d ($\sim$0.5 mM). Another exquisite indicator of chemical exchange is also available through the relaxation properties of the ^{15}N nuclei in the backbone amides by measurement of the T_1, T_2, and heteronuclear nuclear Overhauser effect of the individual sites. Figure 8 shows a plot of these three parameters as well as the ratio T_1/T_2 as a function of sequence position. A total of 106 values out of a possible 126 are considered reliable; gaps occur because of overlap or lack of assignment, and the specific reasons are tabulated in the legend. At this level of analysis the bulk of the residues show regular values of $T_1 \sim 650 \pm 27$ ms, $T_2 \sim 93 \pm 11$ ms, and NOE $\sim 0.80 \pm 0.06$ consistent with a globular protein with a rotational correlation time of 7.8 ns (Kay *et al.*, 1989). However, several sites deviate from this ideality and require additional explanation. Both the C- and N-termini show fast internal motion as evidenced by their longer T_1 and T_2 values and reduced NOE parameters for Lys-4, Leu-127, Gly-128, and Met-129. Lys-91 is even more pronounced in its large-amplitude motion and is between unobserved residues Ala-90 and Lys-92; presumably, these are bleached because of this motion. Several sites in the protein show T_2 values which are below the minimum for the correlation time of the protein, yet have normal T_1 and NOE values; this is most apparent in the T_1/T_2 plot and is due to a chemical exchange mechanism. The most significant deviations occur for Asp-38 and Gly-39, Asn-62 and Asp-64 (unfortunately Met-63 is overlapped and not measured and Pro-61 is not detected), Met-85 and Val-86, and Val-107. All of these residues are in the proximity of the Mg^{2+} binding site (Figure 7), so we attribute the elevated T_1/T_2 to chemical exchange of the magnesium. Further direct evidence for this exchange is that Asp-13, Asn-59, and Gly-65 are only detected in samples containing 30 mM Mg^{2+} and others in this loop are not detected at all because of exchange broadening.

Summary. The assignments and solution structure of the magnesium complex of CheY presented here reveal a structure very similar to those reported by Volz and Matsumura for the magnesium-free form (Volz & Matsumura, 1991) and Stock *et al.* for the magnesium complex (Stock *et al.*, 1989, 1993). Due to exchange broadening caused by the weak and dynamic magnesium binding event, some parts of the structure provide only a few structural constraints and are relatively poorly defined by the NMR data. Nevertheless, the overall global fold is well determined and the α-helices and β-sheet structure agree very well with the crystal structures.

Lys-109 is one of the few residues that is absolutely conserved in the CheY family. In the absence of Mg^{2+}, the Lys-109 side chain forms a salt bridge with the side chain of Asp-57 in the crystal structure. In the crystal structure of the magnesium form (Stock *et al.*, 1993), the side chain of Asp-57 acts as a metal ligand and the salt bridge is broken. Recent studies (Drake *et al.*, 1993; Bourret *et al.*, 1993) with fluorophenylalanine used ^{19}F NMR to monitor structural changes induced by the magnesium binding. These workers observe little change in the ^{19}F chemical shift of Phe-111 and conclude that the salt bridge may still be in place in the magnesium-bound form of CheY. Figure 9 shows a histogram of the distance between the side-chain nitrogen atom of Lys-109 to the closest

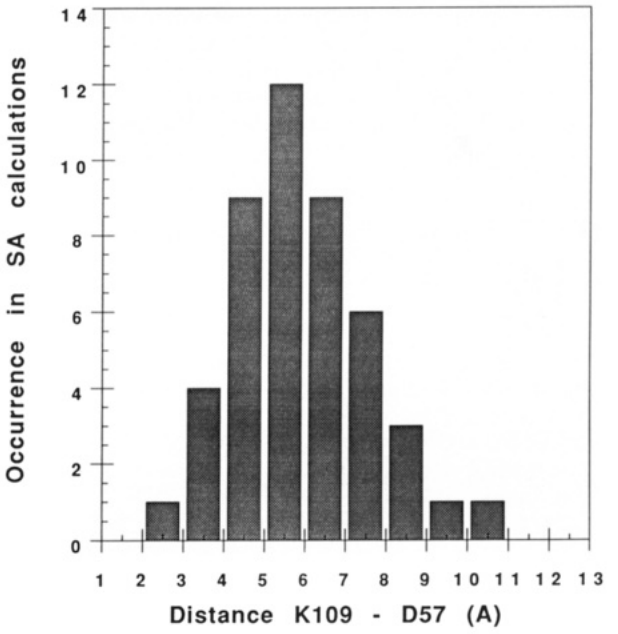

FIGURE 9: Histogram showing the distance between the side-chain carboxylate (closest O) of D57 and the side-chain NH_3^+ of K109 in the final 46 simulated annealing structures; the clustering around a mean distance of 6.0 Å provides convincing evidence for the disruption of the salt bridge in the presence of Mg^{2+} (see text).

oxygen atom of the side-chain carboxyl group of Asp-57 for the 46 simulated annealing NMR structure calculations. In an optimal salt bridge this distance should be 2.8 Å (Anderson *et al.*, 1990), whereas the distance here is centered at 6.0 Å. The dynamics of the backbone ^{15}N–H^N vectors and the number of long-range NOE's show that the structure is quite well-defined in both of these regions of the protein. Moreover, the rms deviation of all atoms in Asp-57 and Lys-109, for an optimally superimposed complete set of backbone atoms, are 1.40 and 1.10 Å, respectively. Taken together, these data provide convincing evidence that in solution the salt bridge is also broken in the presence of magnesium.

ACKNOWLEDGMENT

We thank Wayne Boucher for providing the maximum entropy code and interface, and we appreciate the continuing helpful advice of Ernest Laue on all aspects of the NMR. George Elkins and Gaetano T. Montelione kindly provided the program ORIENT, and Ms. Jean K. Bumby gave helpful comments on the manuscript.

REFERENCES

Anderson, D. E., Becktel, W. J., & Dahlquist, F. W. (1990) *Biochemistry 29*, 2403–2408.
Archer, S. J., Ikura, M., Torchia, D., & Bax A. (1991) *J. Magn. Reson. 95*, 636–641.
Barbato, G., Ikura, M., Kay, L. E., Pastor, R. W., & Bax, A. (1992) *Biochemistry 31*, 5269–5278.
Bax, A., Clore, G. M, Driscoll, P. C., Gronenborn, A. M., Ikura, M., & Kay, L. E. (1990a) *J. Magn. Reson. 87*, 620–627.
Bax, A., Clore, G. M., & Gronenborn, A. M. (1990b) *J. Magn. Reson. 88*, 425–431.
Bax, A., Ikura, M., Kay, L. E., & Zhu, G. (1991) *J. Magn. Reson. 91*, 174–178.
Billeter, M., Braun, W., & Wüthrich, K. (1982) *J. Mol. Biol. 155*, 321–346.
Billeter, M., Neri, D., Otting, G., Qian, Y. Q., & Wüthrich, K. (1992) *J. Biomol. NMR 2*, 257–274.
Bodenhausen, G., & Ruben, D. J. (1980) *Chem. Phys. Lett. 69*, 185–199.

Boucher, W., Laue, E. D., Campbell-Burk, S., & Domaille, P. J. (1992a) *J. Am Chem. Soc. 114*, 2262–2264.
Boucher, W., Laue, E. D., Campbell-Burk, S., & Domaille, P. J. (1992b) *J. Biomol. NMR 2*, 631–637.
Bourret, R. B., Drake, S. K., Chervitz, S. A., Simon, M. I., & Falke, J. J. (1993) *J. Biol. Chem. 268*, 13089–13096.
Brown, S. C., Weber, P. L., & Mueller, L. (1988) *J. Magn. Reson. 77*, 166–170.
Bruix, M., Pascual, J., Santoro, J., Prieto, J., Serrano, L., & Rico, M. (1993) *Eur. J. Biochem. 215*, 573–585.
Brunger, A. T. (1992) *X-PLOR, Version 3.1: A System for X-ray Crystallography and NMR*, Yale University Press, New Haven, CT.
Campbell-Burk, S. L., Domaille, P. J., Starovasnik, M. A., Boucher, W., & Laue, E. D. (1992) *J. Biomol. NMR, 2*, 639–646.
Clore, G. M., & Gronenborn, A. M. (1991) *Annu. Rev. Biophys. Biophys. Chem. 20*, 29–63.
Clore, G. M., Apella, E., Yamada, M., Matsushima, K., & Gronenborn, A. M. (1990) *Biochemistry 29*, 1689–1696.
Clore, G. M., Kay, L. E., Bax, A., & Gronenborn, A. M. (1991) *Biochemistry 30*, 12–18.
Clubb, R. T., Thanabal, V., & Wagner, G. (1992) *J. Biomol. NMR 2*, 203–210.
Drake, S. K., Bourret, R. B., Luck, L. A., Simon, M. I., & Falke, J. J. (1993) *J. Biol. Chem. 268*, 13081–13088.
Gorlach, M., Wittekind, M., Farmer, B. T., II, Kay, L. E., & Mueller, L. (1993) *J. Magn. Reson., Ser. B 101*, 194–197.
Grzesiek, S., Anglister, J., & Bax, A. (1993) *J. Magn. Reson., Ser. B 101*, 114–119.
Havel, T. F., Kuntz, I. D., & Crippen, G. M. (1983) *Bull. Math. Biol. 45*, 665–720.
Ikura, M., Kay, L. E., Tschudin, R., & Bax, A. (1990a) *J. Magn. Reson. 86*, 204–209.
Ikura, M., Bax, A., Clore, G. M., & Gronenborn, A. M. (1990b) *J. Am. Chem. Soc. 112*, 9020–9022.
Ikura, M., Kay, L. E., & Bax, A. (1991) *J. Biomol. NMR 1*, 299–304.
Kabsch, W. (1978) *Acta Crystallogr., Sect. A 34*, 827–828.
Kay, L. E., Torchia, D. A., & Bax, A. (1989) *Biochemistry 28*, 8972–8979.
Kay, L. E., Clore, G. M., Bax, A., & Gronenborn, A. M. (1990) *Science 249*, 411–414.
Kay, L. E., Wittekind, M., McCoy, M. A., Friedrichs, M. S., & Mueller, L. (1992) *J. Magn. Reson. 98*, 443–450.
Kraulis, P. J. (1991) *J. Appl. Crystallogr. 24*, 946–950.
Kraulis, P. J., Domaille, P. J., Campbell-Burk, S. L., Van Aken, T. E., & Laue, E. D. (1994) *Biochemistry 33*, 3515–3531.
Kuszewski, J., Nilges, M., & Brunger, A. T. (1992) *J. Biomol. NMR 2*, 33–56.
Laue, E. D., Mayger, M. R., Skilling, J., & Staunton, J. (1986) *J. Magn. Reson. 68*, 14–29.
Logan, T. M., Olejniczak, E. T., Xu, R. X., & Fesik, S. W. (1993) *J. Biomol. NMR 3*, 225–231.
Lowry, D. F., Roth, A., Rupert, P., Dahlquist, F. W., Moy, F. J., Domaille, P. J., & Matsumura, P. (1994) *J. Biol. Chem.* (submitted for publication).
Lukat, G. S., Stock, A. M., & Stock, J. B.(1990) *Biochemistry 29*, 5436–5442.
Lyons, B. A., & Montelione, G. T. (1993) *J. Magn. Reson., Ser. B 101*, 206–209.
Marion, D., Kay, L. E., Sparks, S. W., Torchia, D. A., & Bax, A. (1989a) *J. Am. Chem. Soc. 111*, 1515–1517.
Marion, D., Ikura, M., Tschudin, R., & Bax, A. (1989b) *J. Magn. Reson. 85*, 393–399.
Marion, D., Ikura, M., & Bax, A. (1989c) *J. Magn. Reson. 84*, 425–430.
Matsumura, P., Rydel, J. J., Linzmeier, R., & Vacante, D. (1984) *J. Bacteriol. 130*, 1317–1325.
Messerle, B. A., Wider, G., Otting, G., Weber, C., & Wüthrich, K. (1989) *J. Magn. Reson. 85*, 608–613.
Montelione, G. T., Wüthrich, K., Burgess, A. W., Nice, E. C., Wagner, G., Gibson, K. D., & Scheraga, H. A. (1992) *Biochemistry 31*, 236–249.
Moy, F. J., Scheraga, H. A., Patt, S. L., & Montelione, G. T. (1992) *J. Magn. Reson. 98*, 451–457.
Moy, F. J., Li, Y.-C., Rauenbuehler, P., Winkler, M. E., Scheraga, H. A., & Montelione, G. T. (1993) *Biochemistry 32*, 7334–7353.
Muchmore, D. C., McIntosh, L. P., Russell, C. B., Anderson, D. E., & Dahlquist, F. W. (1989) *Methods Enzymol. 177*, 44–73.
Neri, D., Otting, G., & Wüthrich, K. (1990) *J. Am. Chem. Soc. 112*, 3663–3665.
Olejniczak, E. T, Xu, R. X., Petros, A. M., & Fesik, S. W. (1992) *J. Magn. Reson. 100*, 444–450.
Powers, R., Garrett, D. S, March, C. J., Frieden, E. A., Gronenborn, A. M., & Clore, G. M. (1993) *Biochemistry 32*, 6744–6762.
Press, W. M., Flannery, B. P., Teukolsky, S. A., & Vetterling, W. T. (1986) *Numerical Recipes*, Cambridge University Press, Cambridge.
Richardson, J. M., Clowes, R. T., Boucher, W., Domaille, P. J., Hardman, C. H., Keeler, J., & Laue, E. D. (1993) *J. Magn. Reson., Ser. B 101*, 223–227.
Seip, S., Balbach, J., & Kessler, H. (1992) *Angew. Chem., Int. Ed. Engl. 31*, 1609–1611.
Shaka, A. J., Lee, C. J., & Pines, A. (1988) *J. Magn. Reson. 77*, 274–293.
Shirakawa, M., Fairbrother, W. J., Serikawa, Y., Ohkubo, T., Kyogoku, Y., & Wright, P. E. (1993) *Biochemistry 32*, 2144–2153.
Spera, S., & Bax, A. (1991) *J. Am. Chem. Soc. 113*, 5490–5492.
States, D. J., Haberkorn, R. A., & Ruben, D. J. (1982) *J. Magn. Reson. 48*, 286–292.
Stock, A. M., Mottonen, J. M., Stock, J. B., & Schutt, C. E. (1989) *Nature 337*, 745–749.
Stock, A. M., Martinez-Hackert, E., Rasmussen, B. F., West, A. H., Stock, J. B., Ringe, D., & Petsko, G. A. (1993) *Biochemistry 32*, 13375–13380.
Stock, J. B., Surette, M. G., McCleary, W. R., & Stock, A. M. (1992) *J. Biol. Chem. 267*, 19753–19756.
Volz, K. (1993) *Biochemistry 32*,11741–11753.
Volz, K., & Matsumura, P. (1991) *J. Biol. Chem. 266*, 15511–15519.
Vuister, G. W., & Bax, A. (1992) *J. Magn. Reson. 98*, 428–435.
Vuister, G. W., & Bax, A. (1993) *J. Am. Chem. Soc. 115*, 7772–7777.
Vuister, G. W., Clore, G. M., Gronenborn, A. M, Powers, R., Garrett, D. S., Tschudin, R., & Bax, A. (1993) *J. Magn. Reson., Ser. B 101*, 210–213.
Wüthrich, K. (1986) *NMR of Proteins and Nucleic Acids*, Wiley, New York.
Wüthrich, K., Billeter, M., & Braun, W. (1983) *J. Mol. Biol. 169*, 949–961.
Zuiderweg, E. R. P., & Fesik, S. W. (1989) *Biochemistry 28*, 2387–2391.